University of Glasgow
DEPARTMENT OF
AEROSPACE
ENGINEERING

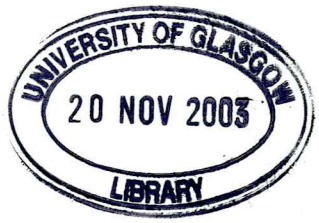

Analysis of Tail Rotor Orthogonal Blade Vortex Interaction.

Dept Report 0301

David R Suttie & Frank N Coton

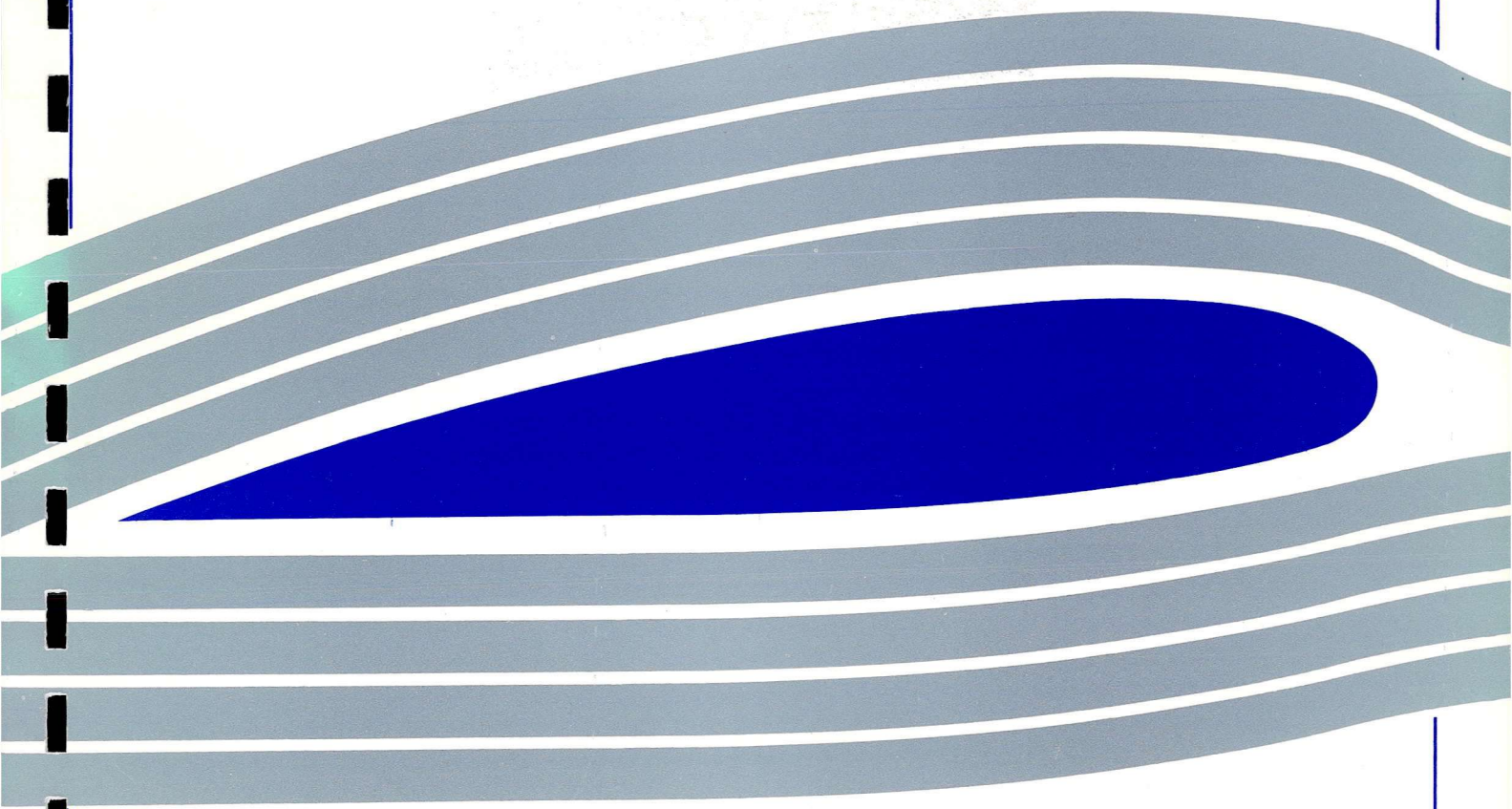

Analysis of Tail Rotor
Orthogonal Blade Vortex Interaction.

Dept Report 0301

David R Suttie & Frank N Coton

Abstract

During helicopter operation, the wake of the main rotor can interact with the main rotor blades and the tail rotor blades. The focus of the present research is the interaction of the main rotor tip vortices with the tail rotor blades. Helicopters are particularly susceptible to this type of blade vortex interaction during low angle descent and climb. As a result of these interactions high decibel noise is emitted and control degradation may occur. The aim of the present research is to indicially model the blade vortex interaction for the limiting orthogonal case. It is hoped that the research will provide a greater understanding of the complex interactions leading, in the long term, to the potential development of more environmentally appealing civil aircraft and increased component life.

In this report initial analysis of pressure data from the orthogonal interactions of a vortex with a stationary blade, collected in the University of Glasgow 2.64 m by 2.04 m wind tunnel is presented. This analysis involved removing high frequency noise and random freestream turbulence effects from the data before examining the impulsive change in normal force during the initial stages of the interaction. It has been established that the impulsive response is most severe in the vicinity of the vortex core centreline where the axial core flow in the vortex is the dominant parameter. With increasing distance from the core, the severity of the response becomes dependent on the sense of rotation of the vortex.

Finally, the future direction of the work towards development of a robust indicial model of the phenomenon is discussed.

Contents

Background

Helicopters are commonly known to produce high levels of noise of a typically broadband nature. However, in some flight conditions there is a strong high frequency impulsive noise that is also generated. Many have investigated this impulsive noise in search of the generator believing the main and tail rotors to be responsible.

In 1987, George and Chou [7] used Amiet's Unsteady Aerofoil theory to show that the frequency of the impulsive noise produced by a helicopter was related to both the main and tail rotor rotational frequencies. George and Chou determined that the acoustics of the tail rotor blade vortex interaction were dependent on the relative location and phasing of the main and tail rotors, and the helicopter flight conditions.

The tail rotor blade vortex interaction's importance as an impulsive noise generator was further highlighted by Samokhin [8], who measured noise levels below a two main rotor setup with the flow impacting on a circular cylinder mimicking a fuselage. He observed that only broadband noise occurred and the impulsive frequencies normally expected to occur were absent, further supporting George and Chou's discovery of the tail rotors' involvement.

Leverton & Pike [18] and Jacobs & Mancini [2], among others, attempted to reduce the impulsive noise levels by altering the design of the helicopter in some way. Alterations included: re-arranging the hub configuration, tip weight, blade thickness, reducing the tip speed, and reversing the tail rotor rotation sense. All resulted in an insignificant reduction of the noise levels generated by the orthogonal blade vortex interaction. They showed that the impulsive interaction could not be easily avoided.

Some have tried to model the impulsive interaction through classical techniques. The studies of Cary [3] and Liou, Komerath & McMahon [9] have highlighted, through failing to model the interaction using classical rigid wake and 2D 'image vortex' concepts respectively, that the interaction has a complex three dimensional nature.

Thus the impulsive interaction has been identified as an interaction between a main rotor's wake and the tail section and blades. The complexity of the interaction is evident from the failure of classical techniques. Also, the avoidance of the interaction is not possible by altering the configuration of the helicopter in the ways attempted by Leverton & Pike and Jacobs & Mancini as previously mentioned.

Orthogonal Blade Vortex Interaction

Depending on the helicopter flight condition, there are several ways in which the tail rotor can interact with the tip vortices trailed from the main rotor. The particular case studied in this report is the orthogonal blade vortex interaction.

In 1987 Cary [3] used oil smoke and stroboscopic photography to visualise the 'cutting' of a vortex by a blade in enough detail to witness changes in the radius of the incident vortex after an orthogonal impact. Since then various researchers have tried to replicate the orthogonal interaction with more success in some cases than others. One of the main problems is the creation of a vortex that is similar to a 'real' helicopter main rotor tip vortex with its associated axial flow.

Since Cary's work in 1987, Johnston & Sullivan [20] replicated the orthogonal interaction observing a more definite distinction of the vortex core behaviour. They observed that on the side of the blade where the axial flow was directed towards the blade, the vortex core size increased. On the opposite side, the vortex core size decreased where the axial flow was directed away from the blade surface. This was observed in surface pressure measurements.

The surface pressure measurements showed pressure and suction peaks illustrating that the short-term blade vortex interaction had occurred. The appearance of pressure and suction peaks indicate that there was vortex axial flow. The pressure peak forms on the side of the

blade where the axial flow is directed towards the blade surface leading to compression taking place, and the suction peak coincides with the axial flow directed away from the blade surface leading to expansion taking place. Therefore the orthogonal interaction can be explained of in terms of the impulsively blocked core axial flow (Doolan [15]).

As previously mentioned Cary [3] used oil smoke visualisation to observe the blade vortex interaction. However, smoke visualisation has problems with implementation, particularly concerning the steady production of the smoke and its entrainment into the vortex core. This results in an imprecise visualisation technique. PIV (particle image velocimetry) offers a much more precise solution.

PIV was used by Doolan [16] and allowed for clarity of most parts of the flow. However, it failed to show flow behaviour within the core due to the high number of 'wild vectors'. Green et al [10] developed an enhanced PIV image processing system that allowed the removal of rogue vectors in the measured flowfield. With this technique a clearer visualisation of activity within the vortex core was achieved.

The vector maps produced by the enhanced processing system allowed visualisation of the radial out-flow on the surface of the blade during the interaction. This occurred on the side of the blade where the axial flow is directed towards the blade, and possibly originated from the vortex core as a direct result of the impulsive blocking of the core flow. There is no radial out-flow at greater distances away from the blade surface.

Marshall in particular has been involved in modelling the interaction numerically as well as conducting visualisation experiments using dyes in fluids. Through his modelling he has ascertained that the impulsive normal force experienced is mainly dependent on the ratio of vortex core radii on opposing sides of the blade.

Marshall used four parameters to define the type of blade vortex interaction that occurs: Impact Parameter, Axial Flow Parameter, Thickness Ratio, and Vortex Reynolds number.

These parameters fully encapsulate the interaction with perhaps the exception of the Thickness Ratio (TR). TR is questionable as it takes into account the ratio of the blade thickness in relation to the vortex size but does not take account of the chord length of the interacting blade. Marshall and his colleagues' have examined the effect of varying these parameters individually.

Krisnamoorthy and Marshall in 1997 [13] highlighted two regimes: a 'weak regime' and a 'strong regime'. An interaction's regime was determined by the value of the Impact Parameter (IP). If the IP was below approximately 0.1 it was defined as a 'strong regime' interaction. If the IP was above approximately 0.25 it was defined as an interaction in the 'weak regime'. Secondary vorticity ejections were observed in both regimes, but in the 'strong regime' secondary vorticity ejections were observed to occur before penetration of the interacting blade into the vortex. However, regime transitions occur gradually and there are a wide range of IP values for which penetration of the blade into the vortex and the secondary vorticity ejections occur simultaneously. These strong and weak regimes were defined for flows where the TR was of order one or less to ensure an impulsive 'cutting' of the vortex occurred.

The behaviour of the secondary vorticity depends on the regime. In the 'weak regime' the secondary vorticity becomes entrained into the core, where as in the 'strong regime' it wraps about the outside of the vortex. The experimental work in Krisnamoorthy and Marshall's [13] paper focused on the strong regime and clearly showed the impulsive interaction in detail and allowed the production of secondary vorticity and this behaviour to be identified. In the 'strong regime' the vortex is strong enough to cause secondary vorticity to be ejected from the blade boundary layer before the impact of the vortex and it was observed to occur earlier for lower IP. The 'strong regime' wrapping process was observed to have the opposite sense to the vortex, which has subsequently been confirmed by other researchers (Affes, Xiao, Conlisk [17]).

The wrapping process, starts off with the formation of multiple vortex threads at different spanwise locations along the leading edge that evolve into a 'sheath' about the primary vortex

with no dramatic (*apparent*) effect on the primary vortex core. The structure of the primary vortex develops depending on the induced velocity of the vorticity threads and the self-induced flow generated inside the vortex core due to the variation in the vortex core's area in response to the secondary vorticity threads. When the vortex core passes the leading edge an eruption of secondary vorticity starts to fill the core on both sides of the blade. This eruption continues after the initial cutting of the vortex, feeding vorticity from the blade boundary layer into the vortex core.

Following this work and using the Ashurst & Lundgren plug flow model for vortex response, Krisnamoorthy and Marshall [19] computationally predicted the formation of a vortex 'shock' (, a discontinuity in core radius,) on the side of the blade where compression from the axial flow takes place. The impulsive interaction compared qualitatively and quantitatively with the increase in core radius on the compression side and a decrease in radius on the expansion side.

In addition to the 'strong regime' and the 'weak regime' defined previously, Marshall and Krisnamoorthy defined a further regime. This occurs when the Thickness Ratio (TR) of the incident vortex is larger than an order of one. In this regime, the vortex stretches about the surface of the blade until the vortex is sufficiently small and close to the blade surface that secondary vorticity is ejected from the boundary layer. Other papers also detail this kind of interaction (Kim and Komerath [14] and Affes & Conlisk [11]).

Also, Marshall explained the behaviour of the secondary azimuthal vorticity by comparing the phase speed, c, of the azimuthal vorticity and the mean axial flow velocity w_0. When w_0 is less than c, the flow is subcritical and upstream-propagating vorticity threads develop. When w_0 is greater then c the supercritical flow does not allow upstream-propagating vortex rings. In the supercritical case the axial flow impinges on the cutting surface like a non-swirling jet would impinge on a flat plate.

Using the Ashurst-Lundgren plug flow model Krisnamoorthy and Marshall determined that a critical value of 0.707 would determine the axial flow regime of a vortex interaction. If the Axial Flow Parameter (AFP) is less than this critical value then the flow is subcritical. In the experimental setup used, the core radius behind the expansion wave decreased as the AFP is increased through the critical region to supercritical flow. On the compression side, the plug flow model predicts the formation of a vortex 'shock' which propagates upstream on the vortex. In subcritical flow a counter-rotating vortex ring forms just upstream of the cutting surface causing the vortex core radius to increase immediately upstream of the vortex location. The vortex ring propagates upstream and leaves weaker vortex rings of alternating sign behind. In the supercritical case upstream-propagating azimuthal vorticity is not possible. After the initial impact the vorticity spreads outward on the cutting surface in the form of a thin propagating sheet of radial and azimuthal vorticity, which is slightly bulged near the leading edge.

Blade vortex interaction has been a source of interest for the University of Glasgow. The university has created vortex generators and tested them with varying vortex size, blade characteristics and wind tunnel sizes. Doolan, in particular, was involved in the initial development of vortex generators and their validation using hot wire anemometry and PIV systems. Green provided more clarity in the complex vortex core region during blade vortex interaction through the use of an enhanced PIV image processing technique mentioned earlier.

Once a stable vortex generator was developed Doolan captured the vortices interaction with a blade at different angles of incidence. The data showed that pressure was increased on the side that was 'exposed' to the axial flow. Doolan observed that changing the angles of incidence did not affect the normal impulsive force experienced by the blade.

Doolan et al [16] observed a nose up pitching moment followed by a nose down pitching moment as the vortex core impacted. Doolan observed the suction peak on the expansion side of the blade travelled and decayed more quickly than the pressure peak on the

compression side. The rapid change in pitching moment towards the expansion side was identified more clearly as the movement of the suction peak past the quarter chord position. Doolan et al, like others, believed that this impulsive loading might be responsible for sound generation and control degradation.

Doolan [16] and Wang [4] completed experimental studies collecting data for multiple angles of incidence and varying freestream velocities. These captured data, along with Doolan's 'stationary blade' data will be analysed and used to build an indicial model.

Data Analysis

The experimental setup in the Argyll Wind Tunnel [2.64m x 2.04m] consisted of a single main rotor blade, rotating in the contraction of the wind tunnel upstream of a stationary blade located in the working section of the wind tunnel. The stationary blade was aligned orthogonally to the freestream flow and the main rotor rotation plane. To ensure the production of tip vortices by the main rotor it was pitched to an angle of 10 degrees for the quarter of the rotation pointing downstream towards the stationary blade. The main rotor was pitched down to 0 degrees during the upwind pass to avoid tip vortex generation. The tip vortices created travelled downstream and interacted with the stationary tail rotor.

The data acquisition system collected data from three parallel pressure transducer arrays mounted flush with the surface of the stationary blade. For each vortex that passed over the stationary blade a block of data was collected by each transducer array. The block contained 2000 data samples at each transducer location covering the time frame that the vortex passed over the blade's surface. A distance of 68.75 mm separated the three transducer arrays and by moving the stationary blade up and down in steps of 20 mm from its original height, data blocks were captured at heights relative to the vortex centre's path at 0 mm: -108.75, -88.75, -68.75, -60, -48.75, -40, -28.75, -20, 0, 20, 28.75, 40, 48.75, 60, 68.75, 88.75 and 108.75 millimetres.

To allow for experimental variations, 16 blocks of data were captured for each of the previously stated relative heights to the vortex centre. This process was repeated for four different freestream velocities (20, 30, 40 and 50 m/s) and thirteen different angles of incidence (from –12 to 12 in increments of 2 degrees) for the stationary blade.

For each freestream velocity the height of the vortex centre was determined by hot wire anemometry as described by Doolan [16] and Wang [4].

Wang developed short programs to convert the data contained in the collected data files. Wang's short programs averaged all 16 data blocks for a transducer array by taking every data 'point' and producing an averaged array for the 2000 data 'points'. By integration of the pressures, this data averaging technique produced Cn (normal force) data which clearly showed the type and general form of the interaction that occurred for each of the transducer arrays for the various angles of attack and the various freestream velocities (See Figure 2).

However, the collected data feature spatial and temporal variations. Ideally, each of the blocks in a 16 block set would experience the impact of the vortex at the same moment because the data collection was synchronized with the vortex generator. However, due to random disturbances in the flow and a small amount of vortex wandering every block experienced the impact at a slightly different time and exhibited a marginally different response.

Due to the spatial and temporal variations, the data created by Wang's algorithm was affected by attenuation. Therefore, to provide a clearer picture of the interaction the magnitude of the dCn (impulsive normal force) event must be established for each individual block of data consequently eliminating the attenuation that occurred.

The impulsive impact of the vortex impacting orthogonally can be clearly seen in nearly all blocks of data. However, the definition of what can be identified as the precise impulsive force is uncertain for two reasons:

1. Naturally occurring random turbulence in the freestream.
2. High frequency background noise.

The impulsive interaction can be determined from the data as a minimum turning point in Cn followed by a maximum turning point in Cn. The detection of this algorithmically is simple, but

the determination of minimum and maximum turning points is not possible if high frequency background noise is present in the data.

Due to the characteristics of the flow the precise value of the impulsive force is hard to accurately quantify. The most obvious solution is to eliminate the high frequency interference with a low band pass digital filter or similar filtering technique. The favoured data analysis package is PV-WAVE, within which it offers three ways to control the interference: a digital filter, splining, or a polynomial fit.

PV-WAVE digital_filter function

When creating a digital filter with PV-WAVE, the function takes 4 parameters, including the low and high frequency cut-offs, the Gibbs phenomenon value, and an nterm value. The Gibbs and nterm values will be discussed shortly.

A suitable filter for these data would remove the high frequency data and hopefully the major oscillations in the Cn curve possibly created by the random disturbances in the freestream. Unfortunately, this required harsh filtering leading to the conclusion that the frequency involved in the interaction was of approximately the same frequency as the interference leading to the impulsive interaction being filtered.

Another observation was made that the filter created by the digital_filter function caused an overall drop in the values of all data points. As the maximum frequency that would be allowed to pass through the filter was lowered there was an amplified distortion of the data. This suggested that the digital filter was efficient up to some performance limits which were not documented.

Adding further lack of confidence in the digital_filter, the PV-WAVE documentation on the precise function and affect of the Gibbs and nterm value were also not documented. The

values appear to control the divergence of the filtered data from the original data. As shown in Figures 3 and 4 the suggested default values for Gibbs (50) and nterm (10) provide the smallest divergence from the original curve. However, with a lack of clear understanding another more straight-forward clean-cut technique was attempted using the spline function.

PV-WAVE spline function

The spline function fills an array with points taken directly from the original data. The plot of the spline data on top of the original data results in a 'join-the-dots' curve fit. Thus all the points in the splined data actually exist in the real data. This is significantly better compared to the unknown accuracy of the digital_filter function. Figure 5 shows an example of splined data on top of dashed original data. Figures 6 and 7 show the splined and original data on their own for comparison.

PV-WAVE poly_fit function

The poly_fit function creates a very loose fit of the original data similar to the digital_filter function. The fit was so loose that the original data may be indistinguishable. The fit did pronounce the impulsive interaction by giving the time frame over which the interaction occurred but with inaccurate start and end times of the interaction. This function was experimented with but the fitting was far too loose and the way in which it was implemented in the built-in procedure was also unknown. The spline function was found to be a much better substitute for both the digital_filter and poly_fit procedures as the way in which the spline functions is simple and its use is straight forward.

Analysis Techniques

Introduction

From the previous techniques for removing high frequency interference the spline technique was the most competent at producing a close fit and still maintaining the magnitude of the original data. The intended technique for analyzing the data was to examine the changing gradients within the data using algorithms written for PV-WAVE. However, the process of identifying the impulsive force is itself debatable and should be discussed before any further analysis takes place.

In the region below the vortex centre line where the local freestream velocity is augmented by the vortex flow, an impulsive interaction is visible. In regions above the vortex centre the impulsive interaction becomes unclear. From the flows where there is a clear impulsive impact sustained from the vortex there is not any conflict in the general consensus on the magnitude of the impulsive interaction. This is true for nearly all the lower and middle array positions. Even though some of the middle array positions may be positioned at locations above the point at which the vortex centre impacts on the blade, it is still possible to determine the dCn (impulsive normal force) magnitude. The lower and middle arrays nearly always show a well-formed impulsive interaction. Figures 8, 9 and 10 show standard graphs created from a data block from the middle, upper and lower transducer arrays.

In some cases the middle array positions feature a more sustained vortex interaction where the normal force increases to a point, levels or drops off in amplitude and then resumes the impulsive increase in normal force again. In these circumstances it is plausible to accept that the full impulsive interaction should be evaluated to the total of the two successive impulsive increases in normal force. Figure 16 graphically shows an example of this assumption.

To control the affect of these lulls in the normal force on the calculation of dCn, a harsh splining technique was employed. Figure 16 shows how 2 small lulls in the impulsive increase

in normal force are evaluated for the whole impulsive interaction. The short dashes indicate the calculated start and end time of the interaction which amalgamate 3 small successive increases in normal force magnitude in to the total impulsive interaction.

Also, in Figure 16 there are two long dashed lines. These indicate the average start and end time of the interaction. To calculate the average, the time period over which the largest impulsive interaction occurred for each of the 16 data blocks of the same interaction was found and then averaged. This average time period was then applied to each data block to find the magnitude of the interaction inside these boundaries.

Before any further analysis is continued some validation of the degree of splining used is required. The high frequency interference is easily controlled by the splining but differing levels of splining affect the control of the random freestream disturbances potentially manifesting as the lulls in the increase of normal force. Since the splining and average time period determination, and its use, are all used purely to obtain the non-dimensional times at which the impulsive interaction actually occurred, harsh splining can be used. The magnitude of the interaction is only taken from the original data after the non-dimensional start and end times of the impulsive interaction for a data block have been obtained.

After testing, an extremely harsh splining technique was employed where the 2000 row original data is reduced to 100 rows. It was found that this level of splining still portrayed the event in the splined data to an extent that most of the random freestream disturbances were 'ignored'. This meant that the 'lulls' previously mentioned could be ignored and counted as the whole impulsive interaction.

With harsh splining, there was the concern that the event that was supposed to be captured would also be 'ignored'. This is not the case with 100 rows as it still describes the interaction to a sufficient degree without masking the time frame when the impulsive interaction occurs. The level of detail still retained in the splined data can be seen in previously mentioned figures (Figures 5, 6 and 7).

As the upper arrays almost always never show any resemblance of interacting impulsively with the vortex the magnitude of the interaction is taken as the change in normal force between equivalent times when the interaction was expected to occur. The equivalent times, referred to as the average start and end times (or the average time period), are calculated from the middle and lower arrays where there is a clear impulsive interaction.

The following section details the process which has led to the development of some acceptable and convincing techniques for the determination of the impulsive force from the data collected in the Argyll Wind Tunnel.

Searching for Minimum to Maximum Turning Points

Once the data has been filtered by PV-WAVE's predefined spline procedure, a procedure for identifying the impulsive normal force (dCn) in the data is required. The typical impulsive normal force observed from the data is a slight drop in normal force followed by a short period of increasing normal force, then a drop in normal force. Therefore a script is required which can find the minimum turning point at the beginning of the event followed by the maximum turning point signifying the end of the event.

The premise of writing an algorithm to search for the minimum and maximum turning points relies on 'smooth' data. The main benefit from filtering the data was to obtain filtered data that would enable a simple algorithm to identify the relevant features of the interaction. The spline procedure gives a very 'jagged' interpretation of the data, but still allows the identification of the main features of the event. The procedure works by looking for a minimum turning point immediately followed by a maximum turning point. This is fruitful with blocks of data from regions on the blade where an obvious impulsive interaction exists.

During testing a stable data set was used, where the angle of attack was 0 degrees and the freestream velocity was 40 metres per second. In this testing data set, clear impulsive interactions were present in all middle array and lower array data blocks over vertical heights, relative to the vortex centre, 108.75 mm below to 40 mm above the vortex centre. For this test data set, vortex radius = 76.3 mm ± 10.24 mm, IP = 15.22, AFP = 0.73, and TR = 0.541 (Wang [21]).

The assumption that the middle and lower arrays contain impulsive interactions has not been tested on the rest of the data. The assumption is useful at this stage for building a technique for calculating the impulsive normal force for all blocks of data by searching for turning points as described above.

Finding the average interaction time period

The following section will detail algorithms attempting to locate the impulsive normal force from the blocks of data. All of the algorithms will use the splined data to locate the average time period over which the interaction occurs, and then returning to the original data to obtain the magnitude of the dCn for the start and end time of the time period previously located. The process is more clearly demonstrated with numbered steps:

1.Find the interaction start and end times for the each of the 16 blocks of data for an array position.
2.Calculate the average of the start and end times for the array position from the 16 blocks.
3.Search for the interaction again inside the average start and end times.

This process is further added to by searching within the combined average of the start and end times found from the lower and middle arrays where a clear impulsive interaction is found. This combined average start time and end time are then used to search within the splined data blocks to find the magnitude of the interaction for the lower, middle and upper

arrays which were captured simultaneously. Therefore the data blocks that feature an impulsive interaction will determine the average time period. After averaging the 16 dCn values calculated for an array position the averaged value is plotted against its relative vertical position to the vortex centre along with the dCn value calculated for the other 16 transducer array positions (between –108.75mm and 108.75mm). This yielded a curve that was close to the anticipated response generated by analyzing Wang's averaged data (Figure 14). Unfortunately there are some problems with this technique.

Obviously, when taking an average, by definition there will be points out with the boundaries defined by the average start and average end times of the time period. Therefore, more often than not, the start or end, or both, will be cut off by these boundaries leading to an incorrect dCn calculation.

When the boundaries for the average time period are defined there still needs to be a technique to obtain the value of the impulsive interaction that often lay just out with the average time period. The best technique to accomplish this by would be to reuse the previous minimum to maximum turning point routine within the average time period. For simplicity this idea was first replaced in the early stages by a simple 'min-max' calculation.

The min-max calculation merely finds the maximum value and the minimum value in the average time period region and assigns the difference as the change in normal force for that data block. This is reasonably effective, but a more accurate calculation could be achieved by a modified version of the minimum to maximum turning point search procedure.

Extension of technique to find average time period

The following technique was developed out of trial and error. The average time period will not inherently include many of the impulsive interactions. However, if the time period was equally stretched in length at both ends degrees of 'generous fits' can be achieved. After extensive

testing a 5% stretch seemed to be appropriate and provided an agreeable calculation of the normal force to the value estimated manually in nearly all cases.

Further to this testing, the possibility of being able to provide a margin of error for each of the interactions could be provided. It was found that an 8% fit would capture every single impulsive interaction in all of the regions where an impulsive interaction was expected. However, in some cases it caught preceding data that was not part of the main event. If a 2% stretch is used then a pessimistic estimate of the impulsive force is achieved. Using stretches in this way provides the possibility of allowing a degree of confidence to be established in the algorithms.

Using the min-max technique along with the extensions of the time periods by 2, 5 and 8 percent results in the following curve (Figure 11). The solid line in Figure 11 shows the result achieved when using the 5 % stretch. Joining the lower error bars shows the pessimistic 2% fit, and joining the upper error bars shows the optimistic 8 % fit.

As the algorithm runs a graph is constructed for every data block indicating the locations of the start and end of the average time period, and the start and end of the impulsive interaction obtained from the procedures previously described. Upon examination of the graphs it was apparent that in most cases where an impulsive interaction was expected to occur the correct value had been obtained. In the other regions, the estimation was not accurate.

To potentially rectify some of the inaccuracy, the min-max procedure was altered. The procedure must now find a minimum value followed by the maximum value in keeping with the assumption that the minimum must be found first before the impulsive interaction occurs. This produced a result that was fairly similar to the previous technique, but it did select more visually pleasing impulsive interactions where the algorithm's selection had previously been inaccurate. Again, the lower error bars represent the 2% fit, the line represents the 5 % fit, and the upper error bars represent the 8 % fit. (See Figure 12.)

A More Sophisticated Impulsive Force Identification (Turning Point)

The min-max technique of obtaining the impulsive force between the average time period is not very sophisticated. Instead of using the min-max routine there is the possibility of re-using the minimum turning point to maximum turning point procedure to identify the magnitude of the impulsive normal force.

The algorithm is altered to allow it to search before the average time period and after it also. The motivation for searching out with these limits is to locate minimum turning points that begin just before the start, or a maximum turning point that lies just after the end of the average time period boundary. This is especially effective for the cases where no obvious impulsive interaction occurs. In these cases the time period over which this occurs is much longer.

As with the algorithm that used the min-max procedure to identify the impulsive normal force inside a time period's boundaries, 2,5 and 8 percent stretches on the time period's boundaries were implemented. As expected the percentage stretches frequently results in the same dCn result. This occurs because the searching out with the time period's boundaries is permitted. The most common location this occurs is when there is a clear, well-formed impulsive interaction. When this happens it signifies a confident identification of the location and magnitude of the impulsive normal force interaction.

When this technique tries to interpret the regions where an obvious impulsive interaction does not occur a confused graph is obtained. In regions where the flow is transient between flows that contain an obvious impulsive interaction and those that do not, then adjacent impulsive events may be identified because of the different percentage stretches. This can lead to the situation where the varying stretches applied to the time period boundaries result in events of similar magnitude being identified, and in the some cases both events should have been summed.

This illustrates the fact that it is difficult to decide what the impulsive interaction is in the area above the vortex centre both by manual interpretation and by computational analysis. The result of reusing the turning point techniques can be seen in Figure 13.

Summary of Analysis Techniques

The techniques discussed provide some good quality resolution of the interaction for vortex heights where an impulsive interaction is obvious. dCn is hard to define manually or computationally, as there is no appreciable impulsive interaction in the flow region where the freestream velocity is not augmented by the vortex. Both the min-max and the minimum to maximum turning point techniques give good results for the compressed flow regions where augmentation by the vortex occurs.

The turning point technique sometimes gives inconsistent results. In some cases it will, due to searching outside the average time period boundaries, evaluate the interaction to a long slow interaction more in common with the circulatory interaction that takes place. Analyzing the data using the min-max technique does force the declaration of a data blocks impulsive interaction to be confined to the time period that it occurs over.

Both techniques, min-max and turning point, ultimately illustrate the non-existence of a 'clear-cut' impulsive interaction away from the vortex centre in the expansion region at distances similar and greater than the calculated vortex's core radius.

To confirm the validity of the technique the graphs were compared against the output obtained from Wang's straightforward averaged data. The graphs compare favourably and also demonstrate that attenuation did occur with the averaged data created by Wang's script. Graphs showing the comparison between the original 'min-max', the improved 'min-max', the

turning point technique, and analysis of Wang's averaged data can be found in Figures 11,12,13,14 respectively.

Future Work - dCn analysis

A vortex's path is difficult to control. Frequently the vortex will wander from the intended path. In the data captured by Wang, it can be discerned, analyzing the data from each of the three transducer arrays, that the vortex impacts at a slightly different height in each of the 16 data blocks. By analyzing the 3 interactions experienced by the 3 transducer arrays it may be possible to find the exact vortex height at which each vortex interacted with the blade.

After establishing the average trends from the actual data and also the trends from Wang's 'averaged' data, it may be possible to examine data from the three measurement arrays and fit their position to the curve of the vortex height against the magnitude of the vortex interaction. This will allow the identification of the vortex centre height in each block. Processing middle and lower arrays would be fairly straight forward, but the upper arrays would potentially cause a problem as they typically contain no clear-cut impulsive interaction. This technique may not yield a clear image of the interaction if it is not the vortex drifting but the random freestream disturbances that are causing the appearance of vortex drifting in the data.

Future Work – Indicial Modelling

Using the collected data as a template, the initial stages of indicially modelling the interaction have started. The use of Kussner and Wagner functions in response to vertical gusts and step changes in angle of attack respectively, are currently being incorporated and the functions will be combined to represent the form of the interaction found in the collected data.

References

1. Copland, C.M., Coton, F.N., Galbraith, R.A.McD., "A Study of Helicopter Tail Rotor Interaction: Phase 1: Proof Of Concept", *24th European Rotorcraft Forum*, 1998.
2. Jacobs, Eric W., Mancini, John, Visintainer, Joseph A., Jackson,Tracy A., "Acoustic Flight Test Results for the Sikorsky S-76 Quiet Tail Rotor at Reduced Tip Speed", *American Helicopter Society*, 53rd Annual Forum, 1997.
3. Cary, Charles, "An Experimental Investigation of the Chopping of Helicopter Main Rotor Tip Vortex by the Tail Rotor, Part II: High Speed Photographic Study", *NASA Contractor Report 177457*, 1987.
4. Wang, Tongguang, Doolan, C. J., Coton, F.N., Galbraith, R.A.McD., "An Experimental Study of the Three-Dimensionality of Orthogonal Blade-Vorex Interactions with a Stationary Blade", (in publication).
5. Wang, Tongguang, Doolan, C. J., Coton, F.N., Galbraith, R.A.McD., "An Experimental Study of the Three-Dimensional Vortex Interactions with a Rotating Rotor", (in publication).
6. Lundgren, T.S., Ashurst, W.T., "Area-varying Wave on Curved Vortex Tubes with Application to Vortex Breakdown", *Journal of Fluid Mechanics*, 1989.
7. George, Albert R. and Chou, S.-T. "Helicopter Tail Rotor Blade-Vortex Interaction Noise", *NASA Ames Research Center*, 1987.
8. Samokhin, V.F., "Impulsive Noise of Helicopter Tail Rotor", *21st European Rotorcraft Forum Paper I.6*, 1995.
9. Liou, S., Komerath, N., McMahon, H., "Measurement of Transient Vortex-Surface Interaction Phenomena", *AIAA Journal 89-0833*, 1989.
10. Green, R.B., Doolan, C.J., Cannon, R.M., "Measurements of the Orthogonal Blade-Vortex Interaction using the PIV Technique", 2000.
11. Affes, H., Conlisk, A.T., "Model for Rotor Tip Vortex-Airframe Interaction, Part I: Theory", *AIAA*, 1993.
12. Doolan, C.J., Coton, F.N. And Galbraith, R A McD, "Normal Vortex interaction with A Loaded Symmetrical Blade", *25th European Rotorcraft Forum*, Paper No C2.

13. Marshall, J.S and Krisnamoorthy, S. ,"On the Instantaneous Cutting of a Columnar Vortex with Non-Zero Axial Flow", *J Fluid Mech*, 1997, 351, pp41-74.

14. Kim, J.M., Komerath, N.M., "Summary of the Interaction of a Rotor Wake with a Circular Cylinder", *AIAA Journal Vol. 33 No. 3*, 1995.

15. Doolan, C.J., Coton, F.N. And Galbraith, R A McD, "Surface Pressure Measurements of the Orthogonal Vortex Interaction", *AIAA Journal*, Vol. 39, No. 1, 2001.

16. Doolan, C.J., "Surface Pressure Measurements of Three-Dimensional Vortex Interactions with a Stationary Blade", ???

17. Leverton, John W., Pike, Tony C., "The Importance of Tail Rotor Interaction as an Acoustic Source", *American Helicopter Society*, 1993.

18. Krishnamoorthy, S. and Marshall, J.S. ,"Three-dimensional Blade Vortex Interactions in the Strong Vortex Regime", *Physic of Fluids*, 1998, 10, (11), pp2828-2845.

19. Johnston, R.T. And Sullivan, J.P., "Unsteady Wing Surface Pressures in the Wake of a Propellor", *AIAA Paper 92-0277*, AIAA Aerospace Sciences Meeting, Reno, USA, January 1992.

20. Rockwell, Donald, "Vortex-Body Interactions", *Annual Review of Fluid Mechanics*, 1998.

21. Marshall, J.S., "Vortex Cutting by a Blade, Part I: General Theory and a Simple Solution", *AIAA Journal Vol. 32 No. 6*, 1994.

22. Marshall, J.S., Yalamanchili, R., "Vortex Cutting by a Blade, Part II: Computations of Vortex Response", *AIAA Journal Vol 32 No 7*, 1994.

Figures

Figure 1

This figure shows a standard data block captured showing an impulsive change in normal force as the vortex passes over the blade.

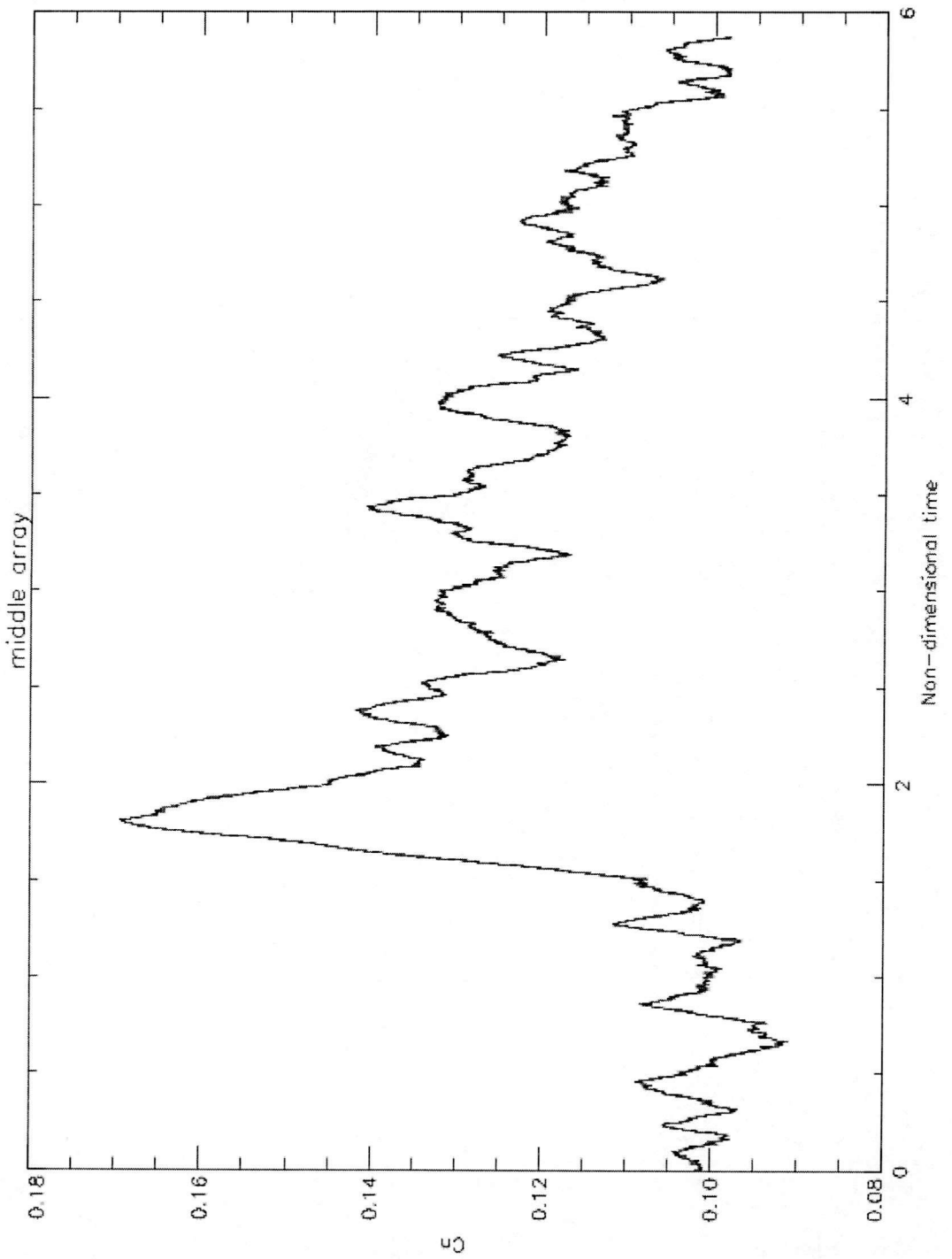

Figure 2

This figure shows the output obtained when using Wang's averaging technique. This data is attenuated but still shows the general form of the interaction.
Graph also shows the identification of the impulsive interaction by the algorithm.
Long dashes indicate the average time period and short dashes indicate the start and end times of the calculated impulsive interaction.

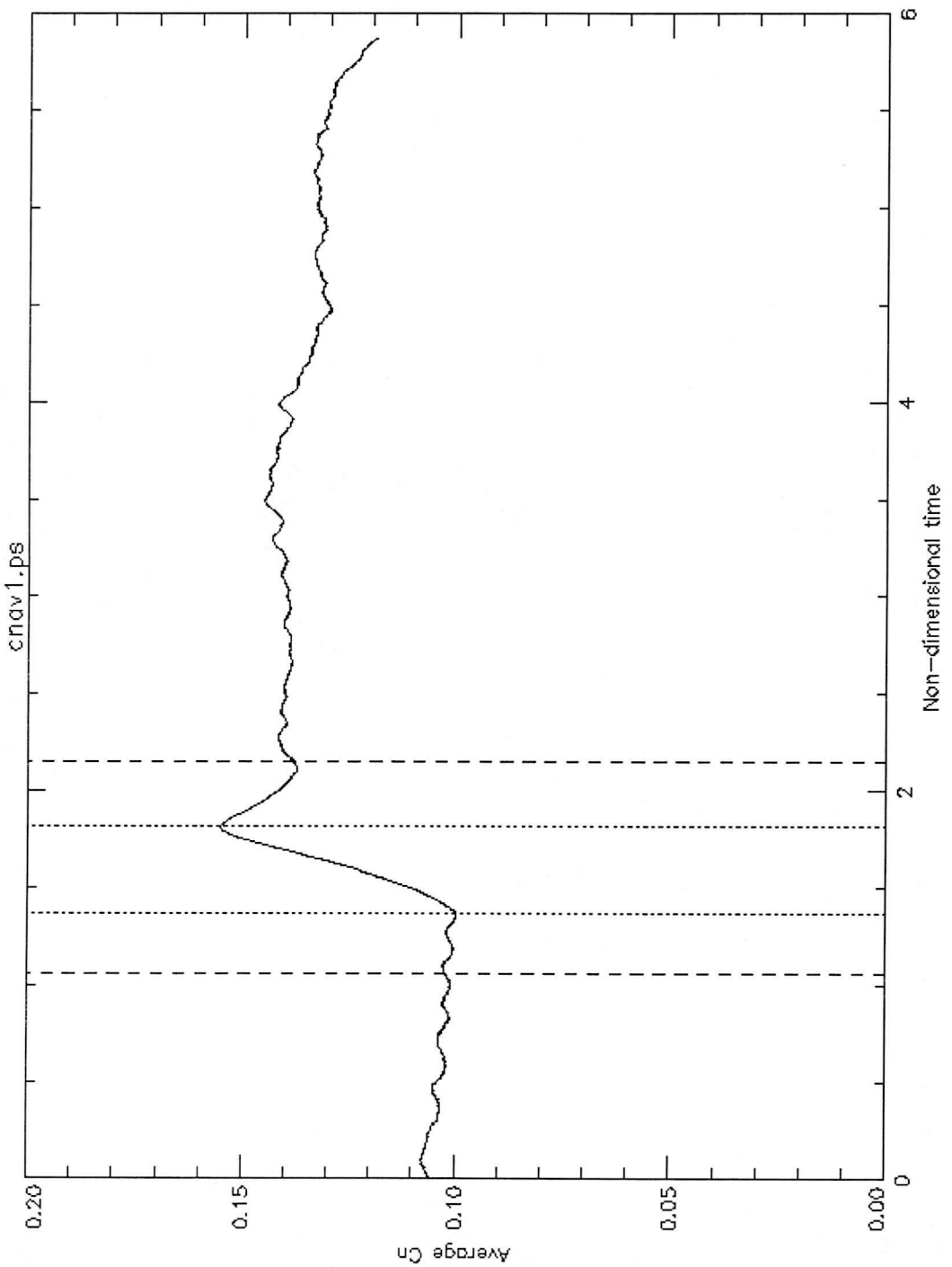

Figure 3

This figure illustrates the distortion caused by varying the Gibbs value in PV-WAVE's digital filter. The average distortion from original signal is plotted.
This curve is created using the default value for nterm of 10.

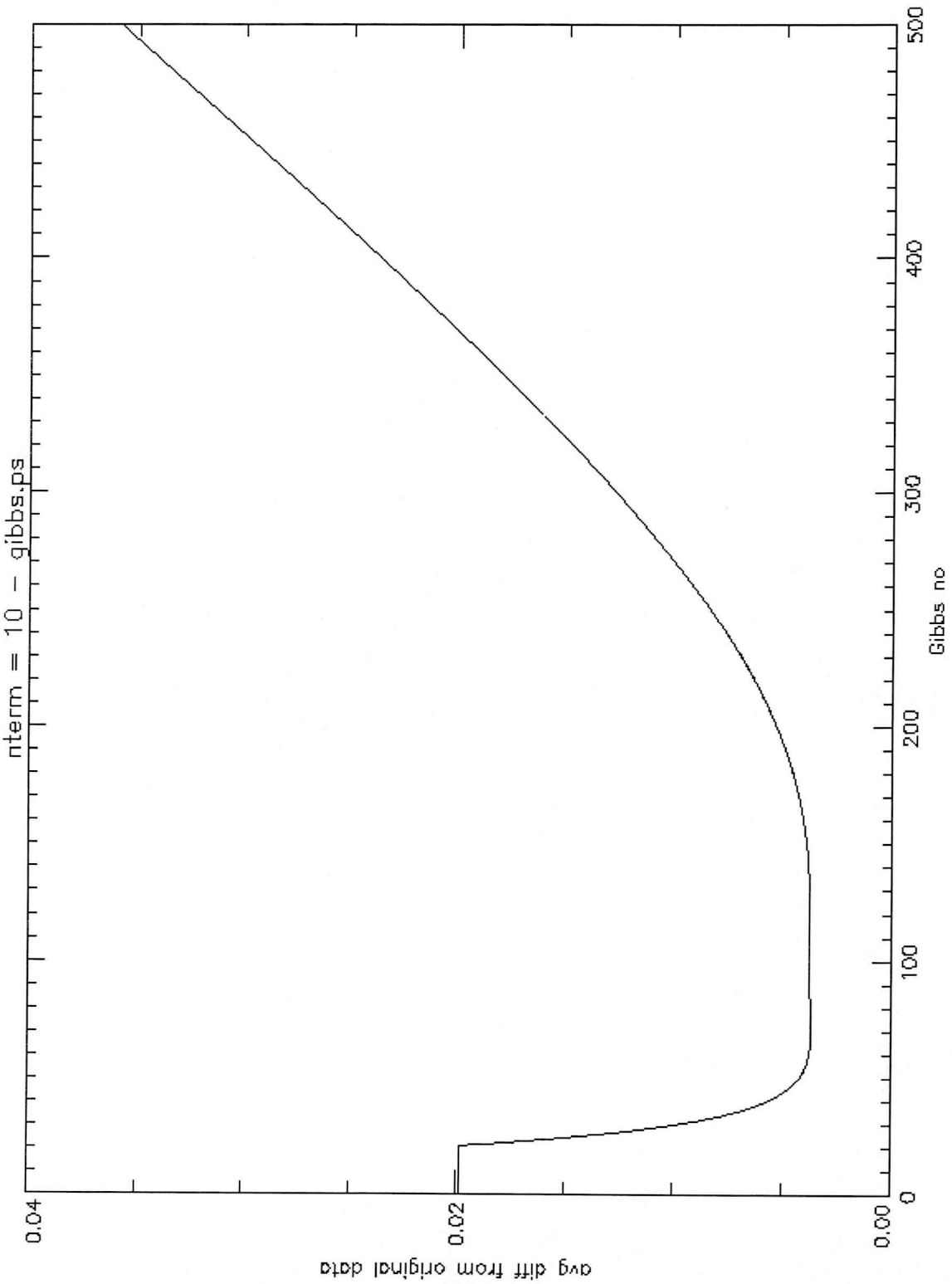

Figure 4

This figure illustrates the distortion caused by varying the nterm value in PV-WAVE's digital filter. The average distortion from original signal is plotted.
This curve is created using the default value for Gibbs of 50.

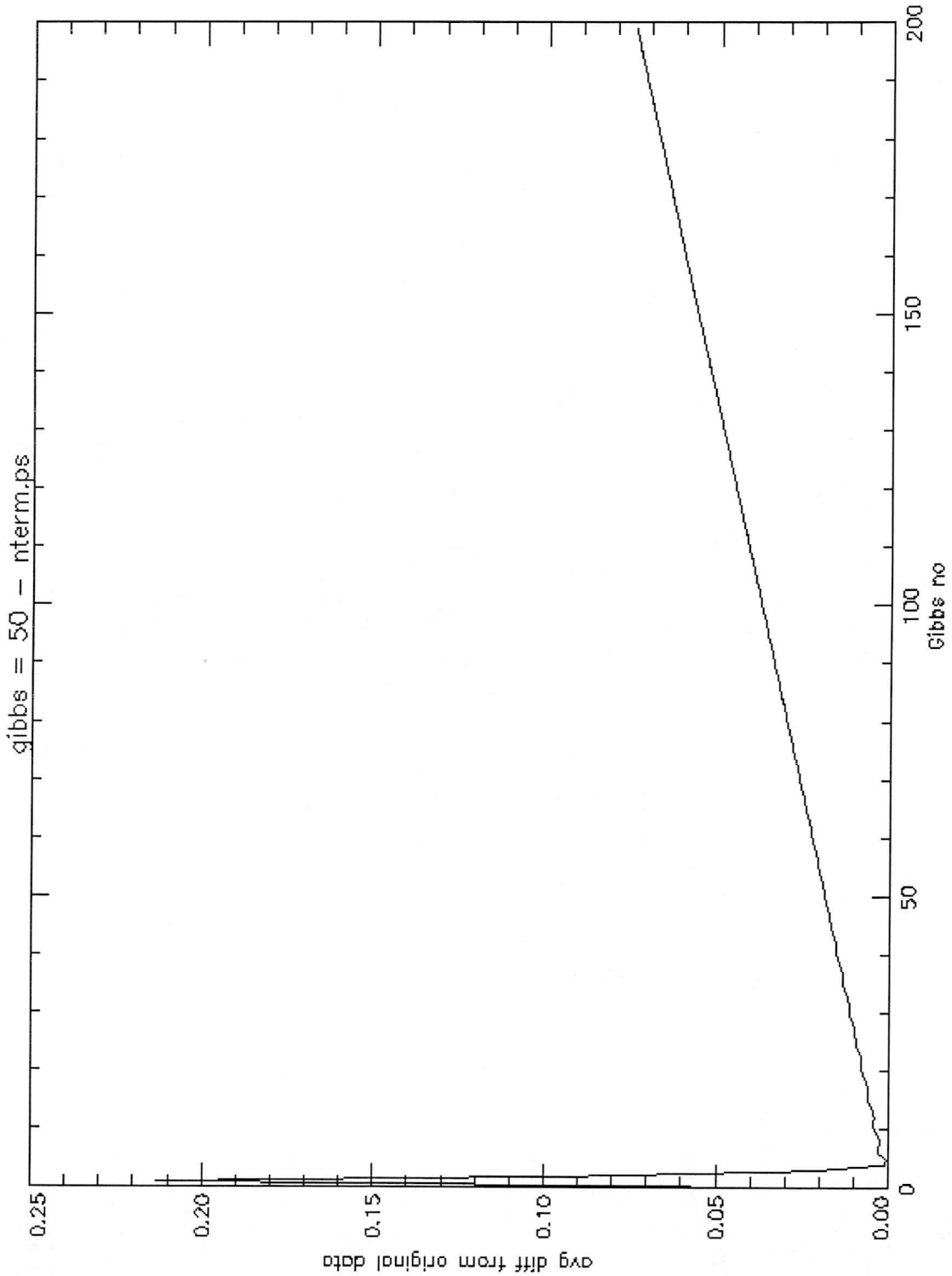

Figure 5

This figure allows the comparison of the splined data and the original data to be visualised. The splined data is the solid line and the original data is the dashed line.

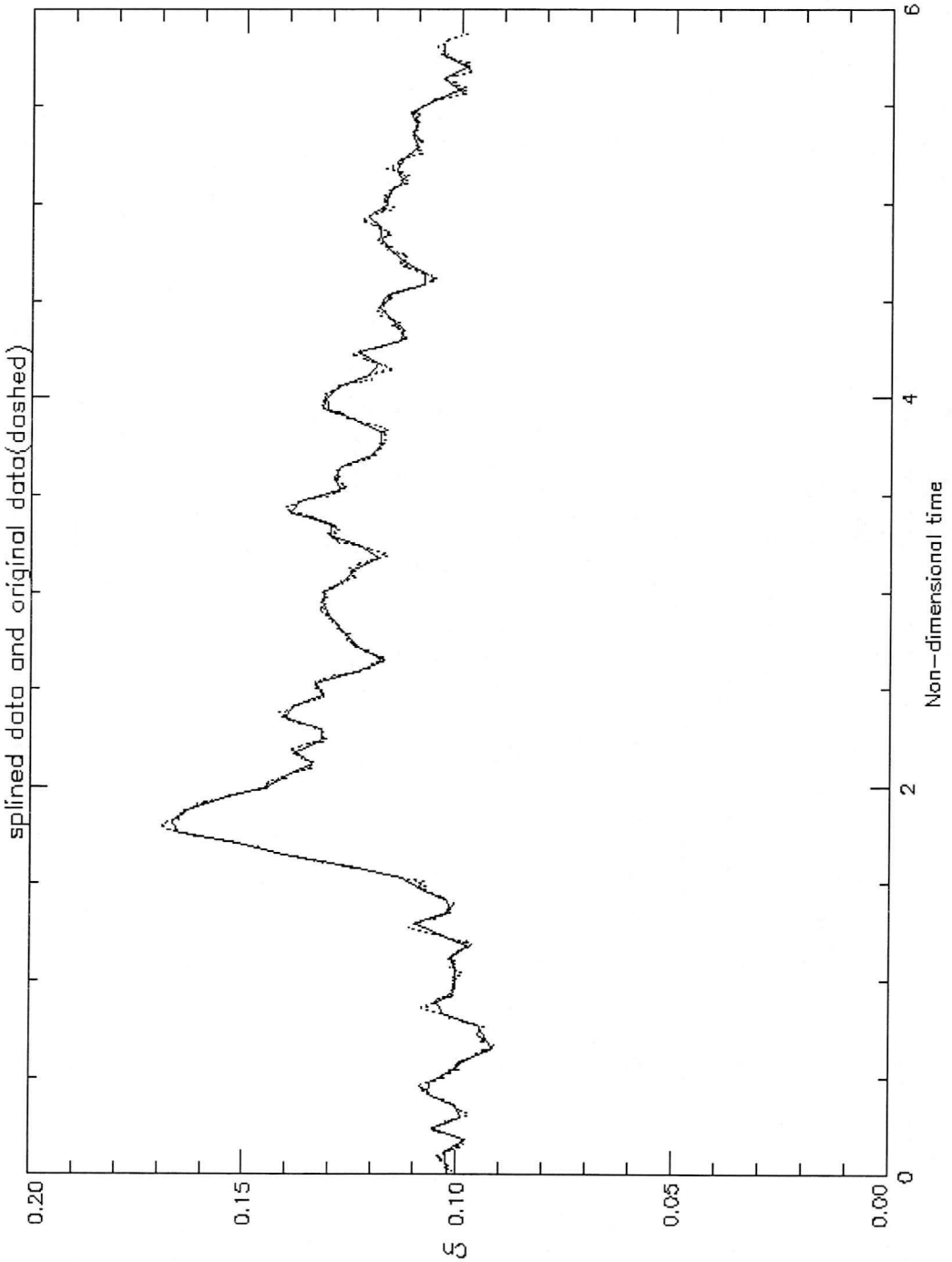

Figure 6

This figure shows the splined data from Figure 5.

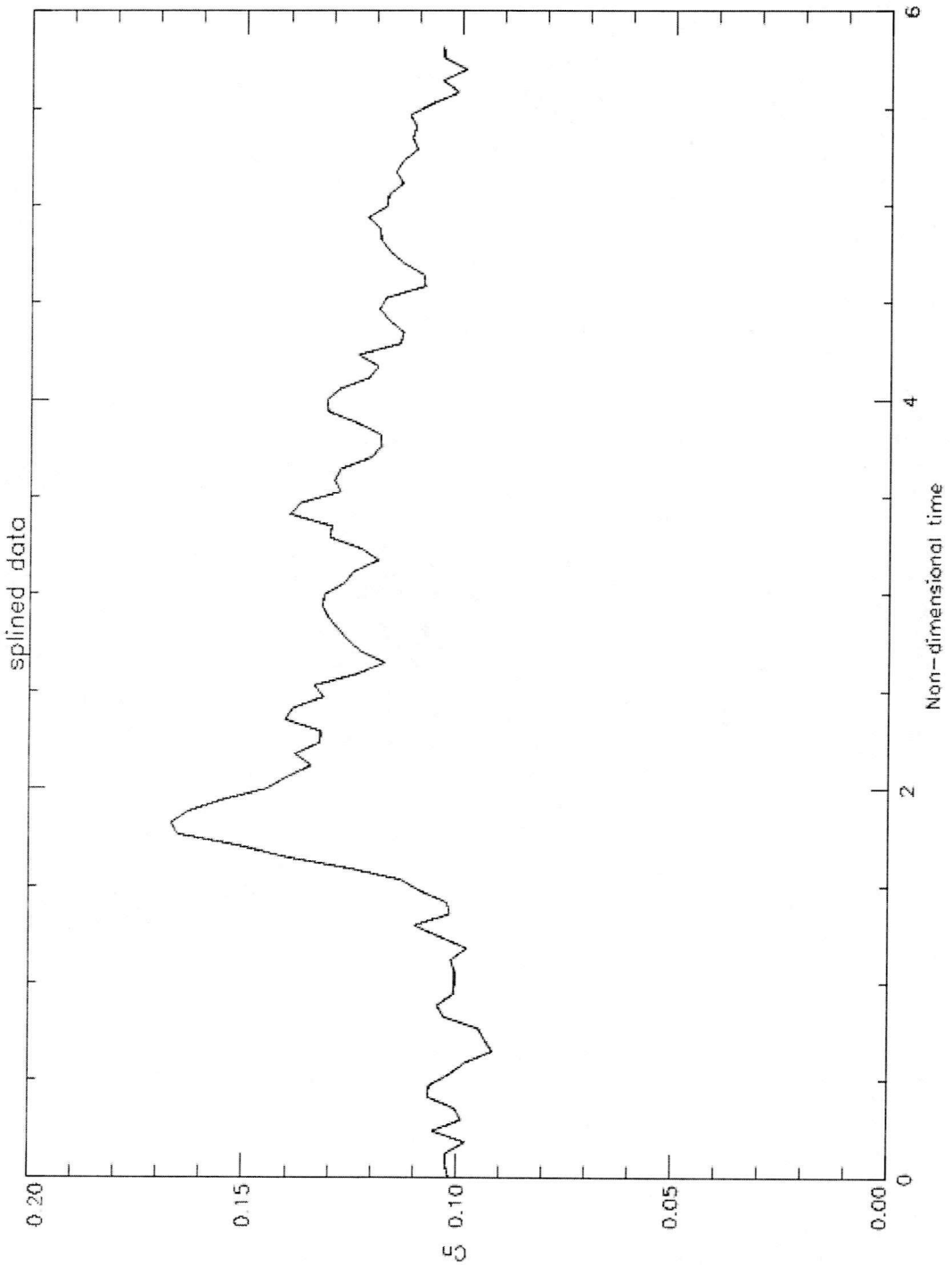

Figure 7

This figure shows the original data from figure 5.

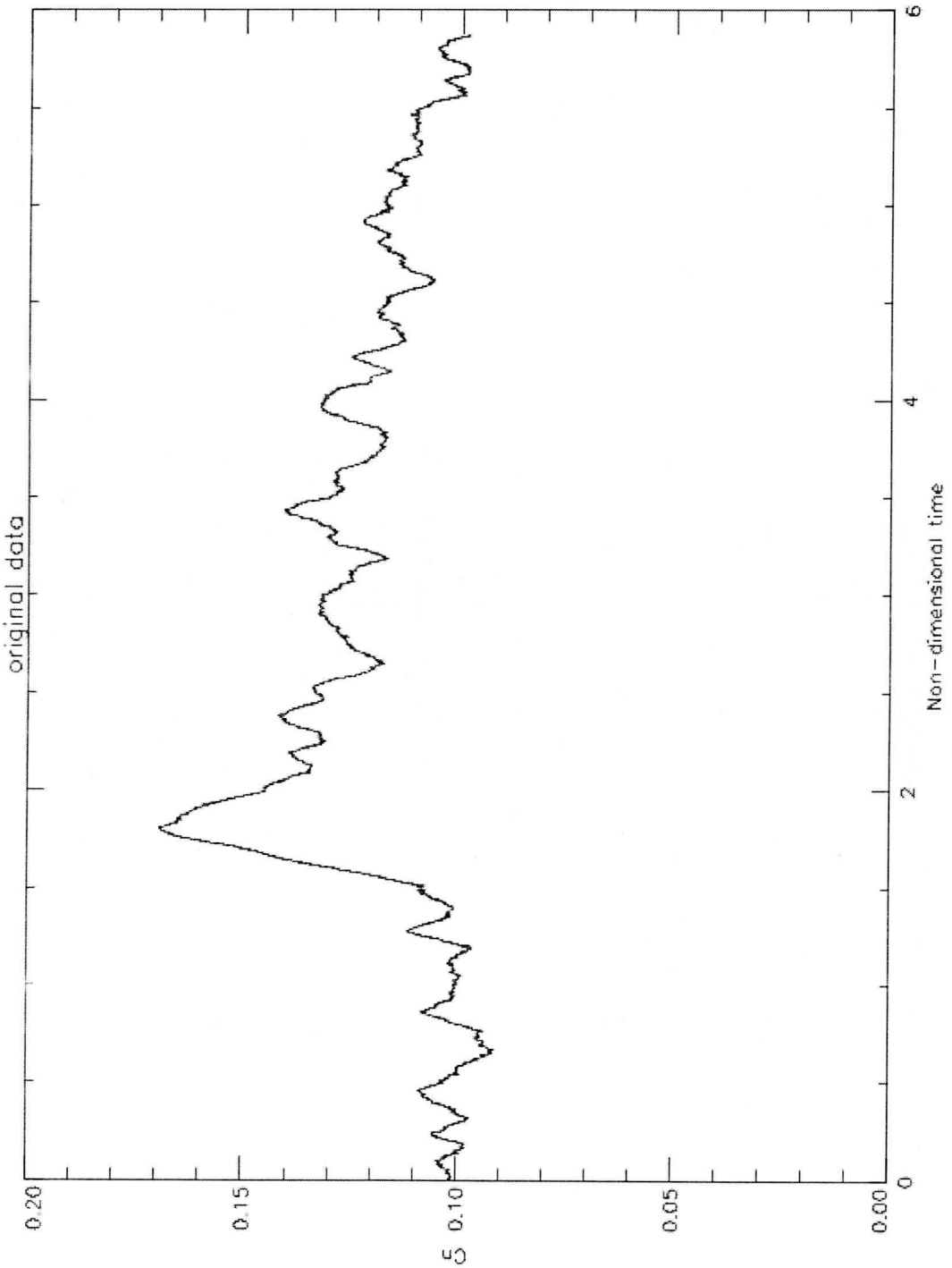

Figure 8

This figure shows a typical data block collected from a middle transducer array.

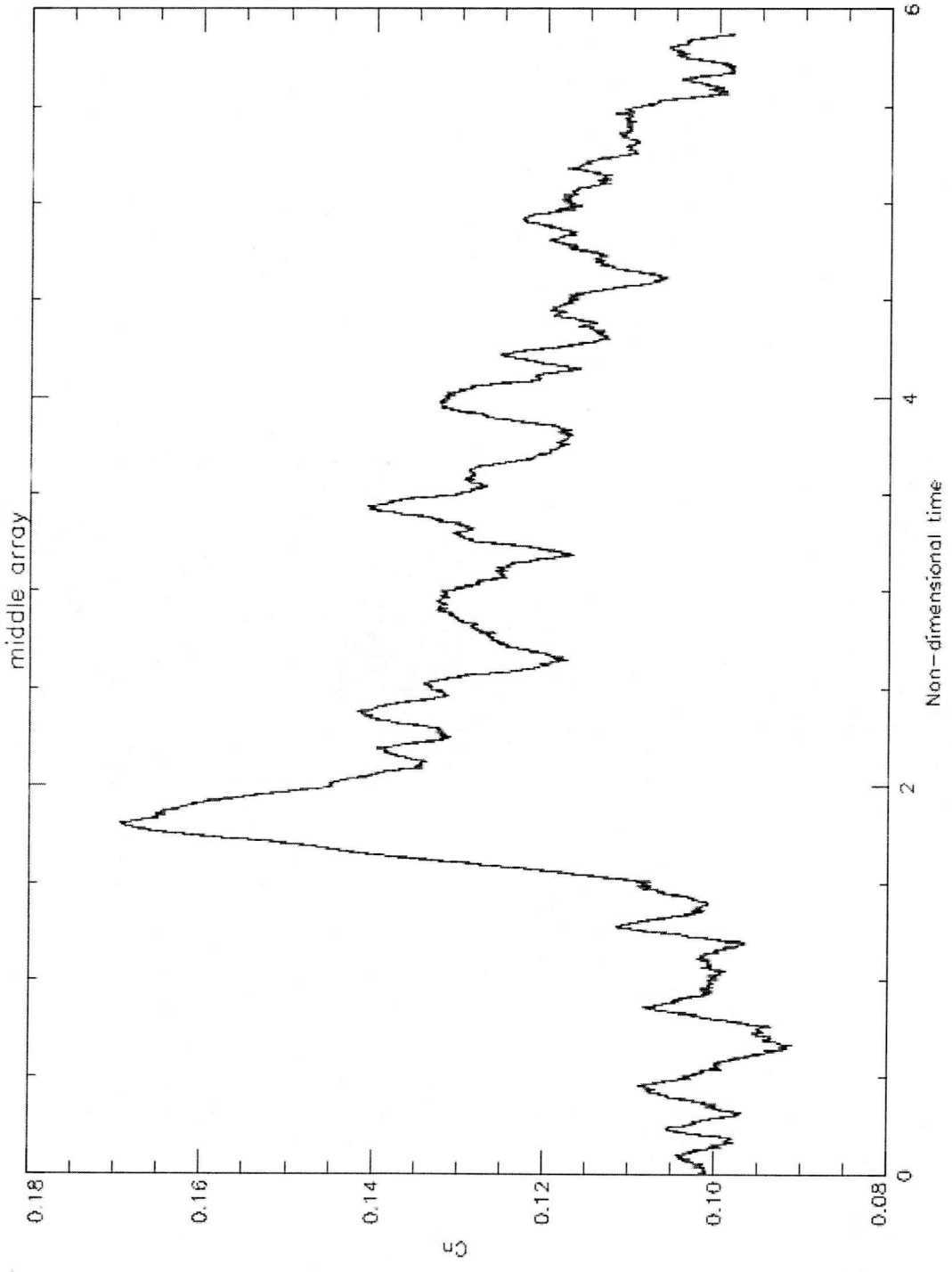

Figure 9

This figure shows a typical data block collected from an upper transducer array.

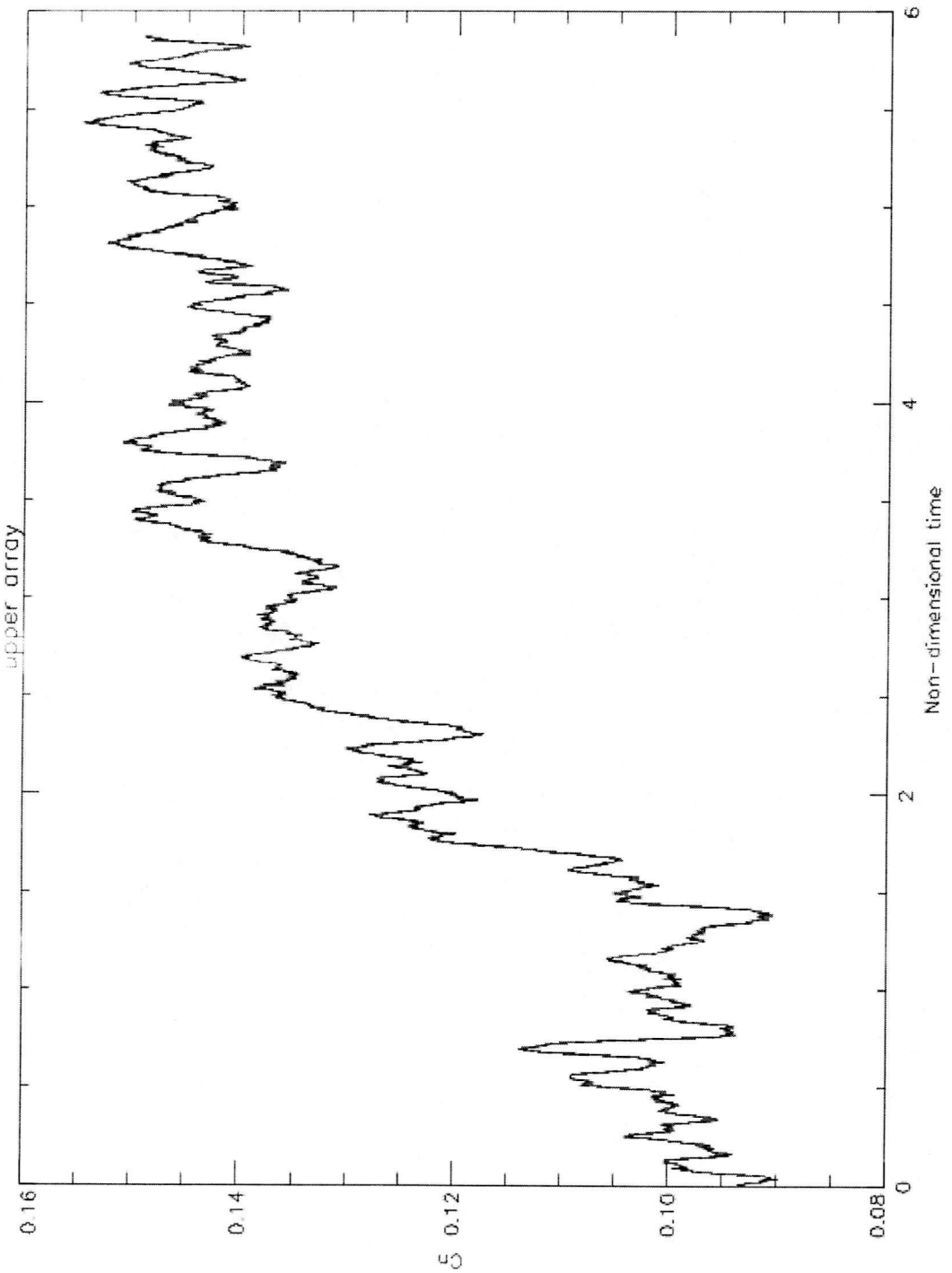

Figure 10

This figure shows a typical data block collected from a lower transducer array.

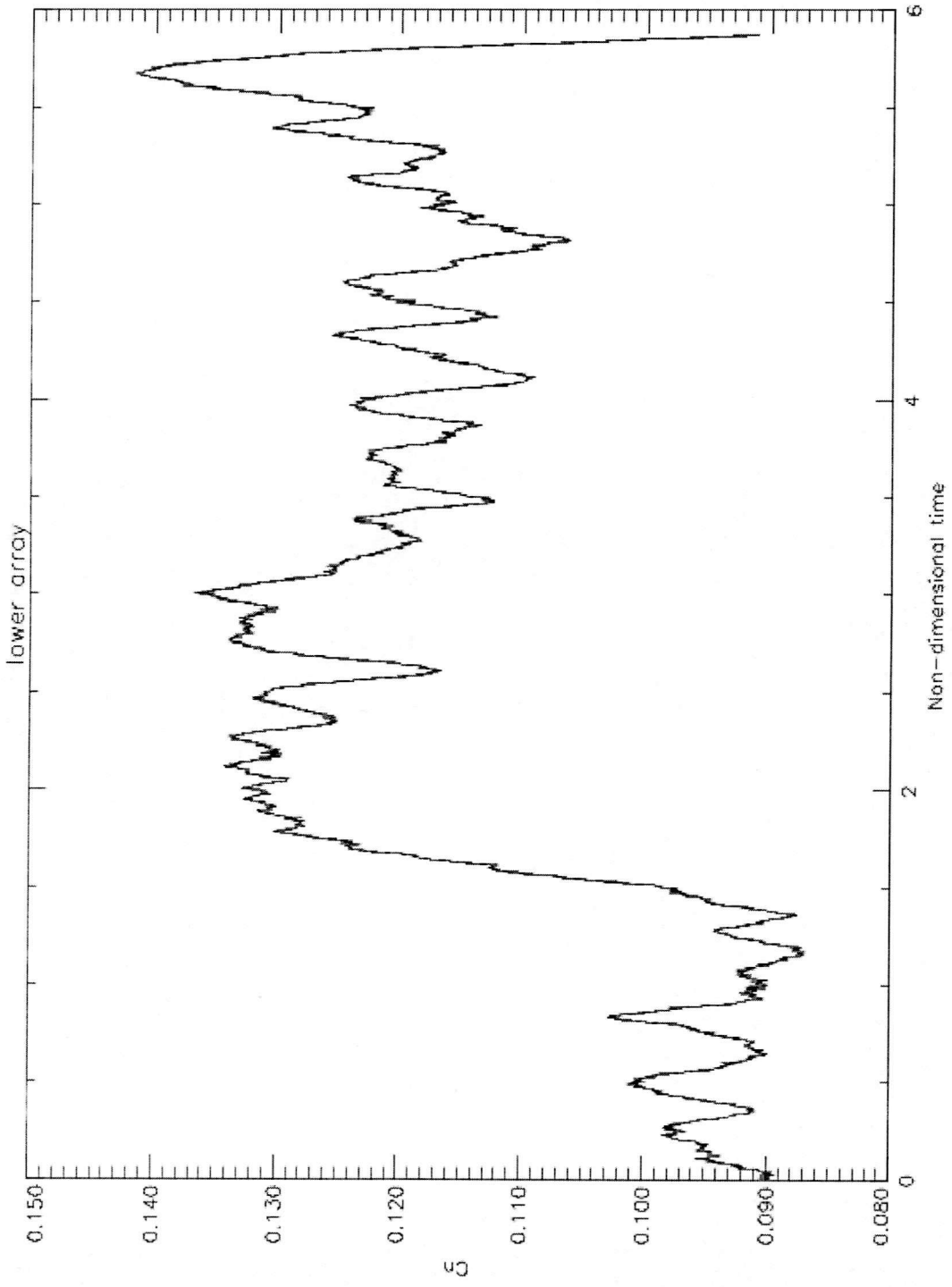

Figure 11

This figure shows the output obtained from the original 'min-max' technique.
The solid line represents the 5% stretch fit.
The lower error bars represent the 2% stretch fit and upper error bars the 8% fit.

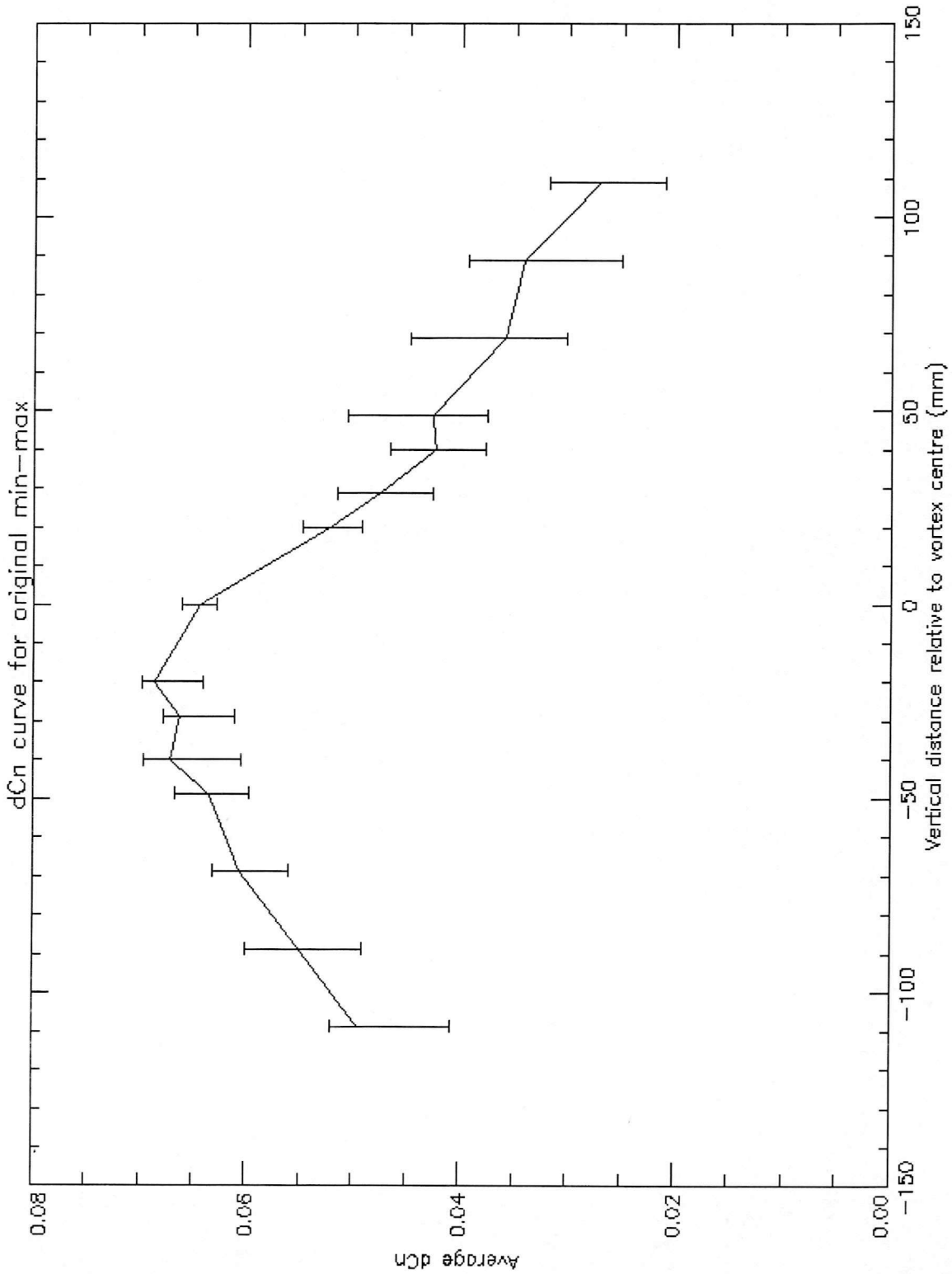

Figure 12

This figure shows the output obtained from the improved 'min-max' technique.
The solid line represents the 5% stretch fit.
The lower error bars represent the 2% stretch fit and upper error bars the 8% fit.

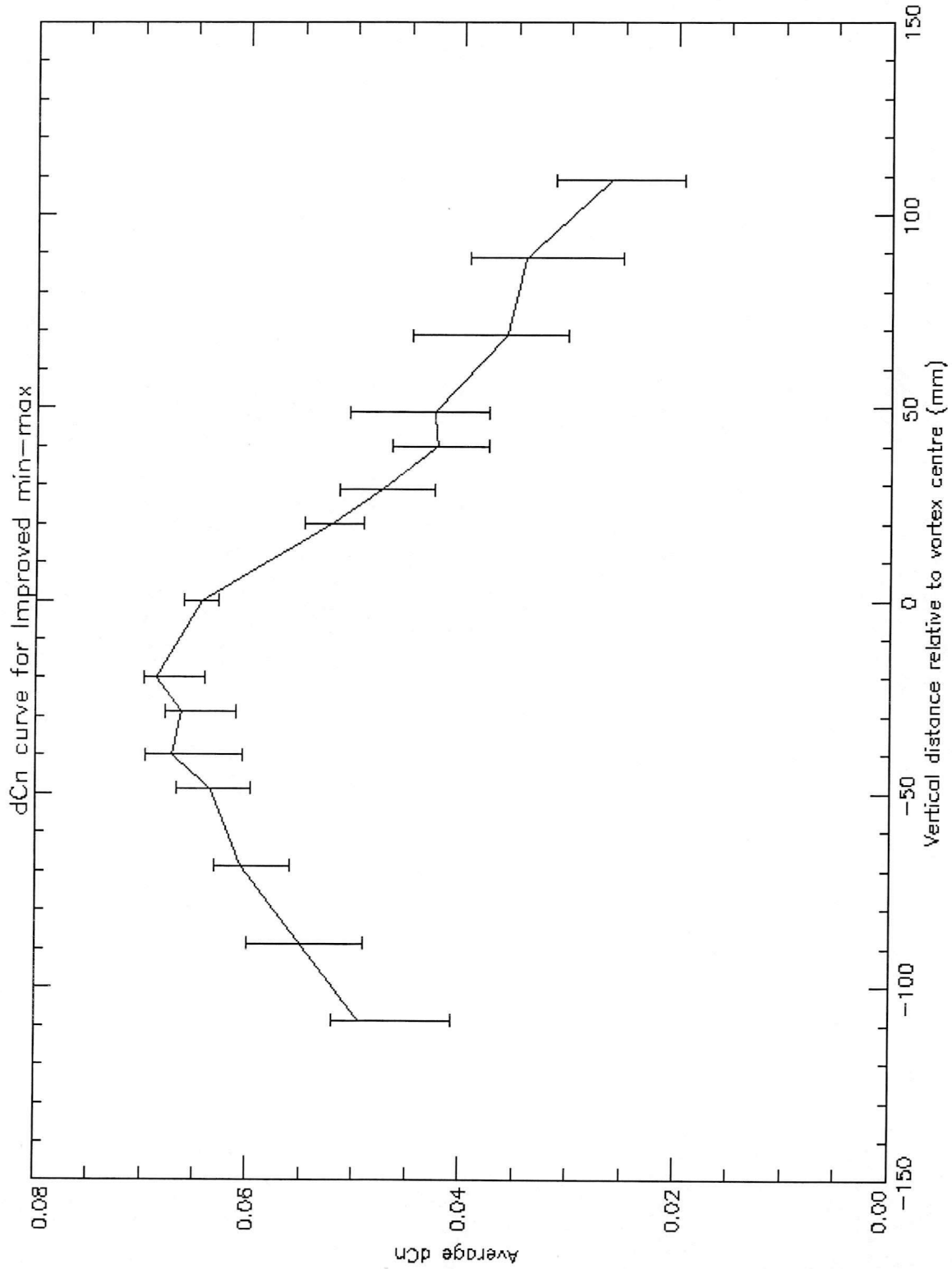

Figure 13

This figure shows the output obtained from the turning point technique.
The solid line represents the 5% stretch fit.
The lower error bars represent the 2% stretch fit and upper error bars the 8% fit.

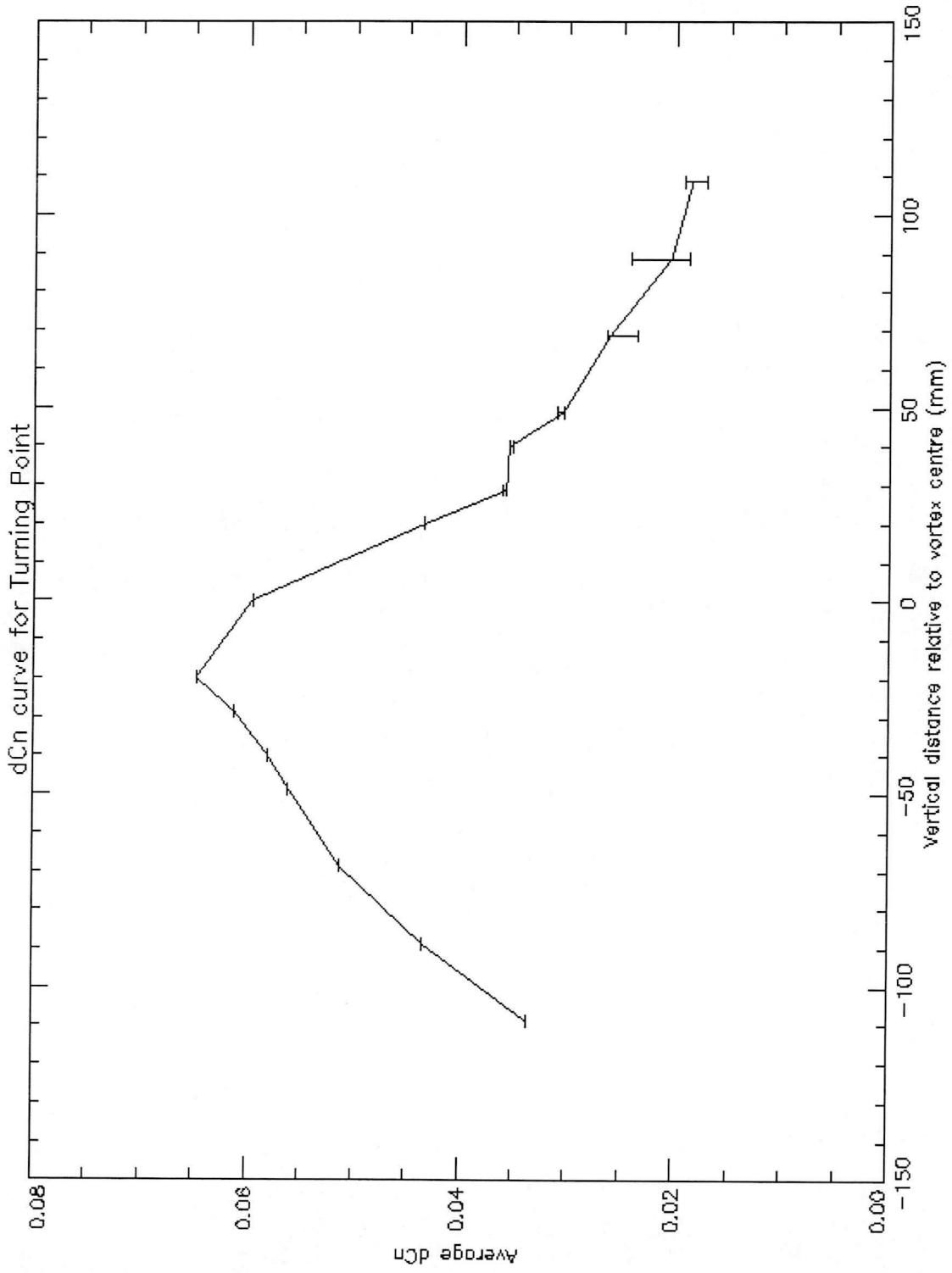

Figure 14

This figure shows the output obtained from analysing Wang's averaged data.
The solid line represents the 5% stretch fit.
The lower error bars represent the 2% stretch fit and upper error bars the 8% fit.

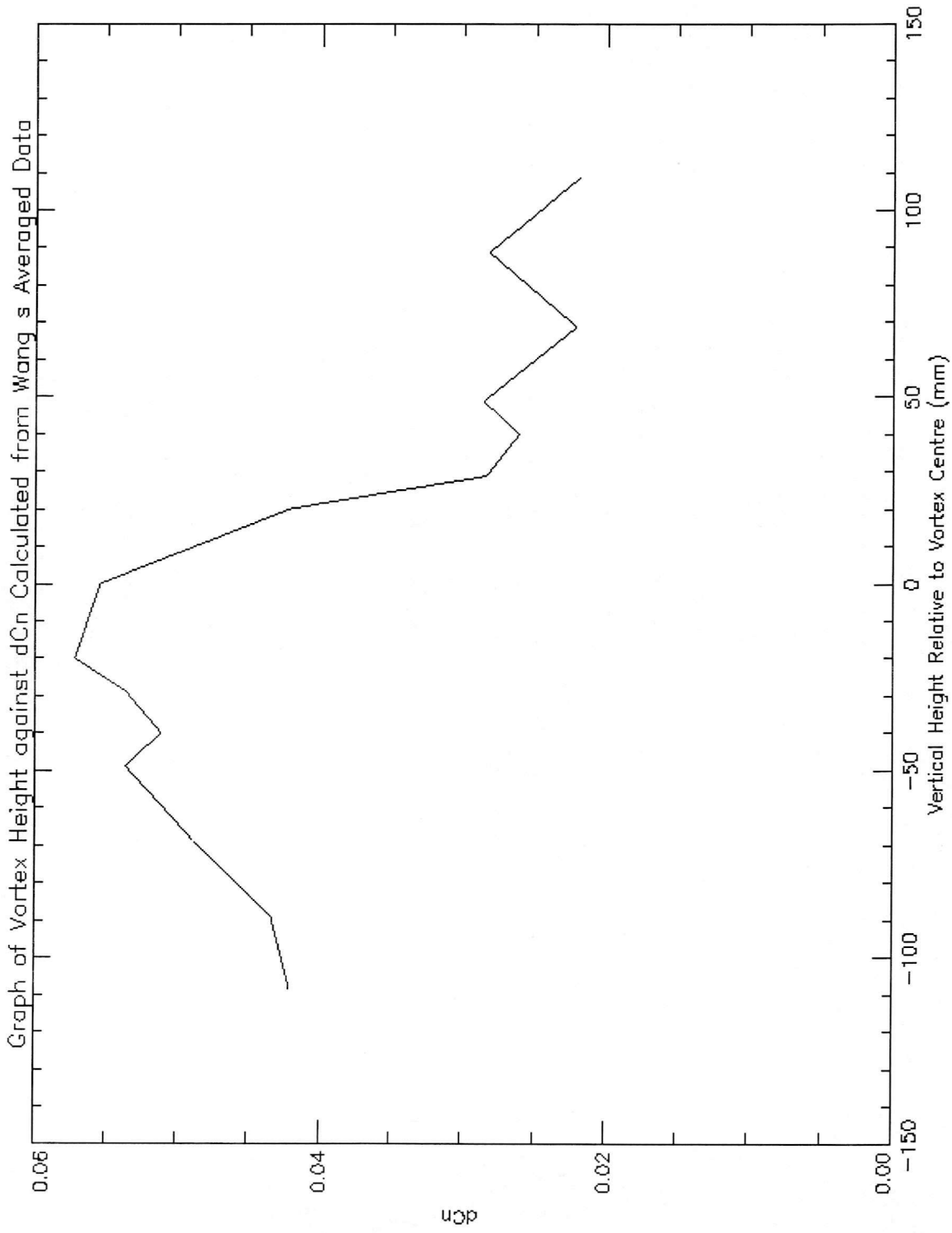

Figure 15

This figure shows the extent of a 2 % stretch of the average time period in comparison to Figures 16 and 17.
The long dashes indicate the average time period and the short dashes indicate the points taken as the start and end of the impulsive interaction with the original 'min-max'.

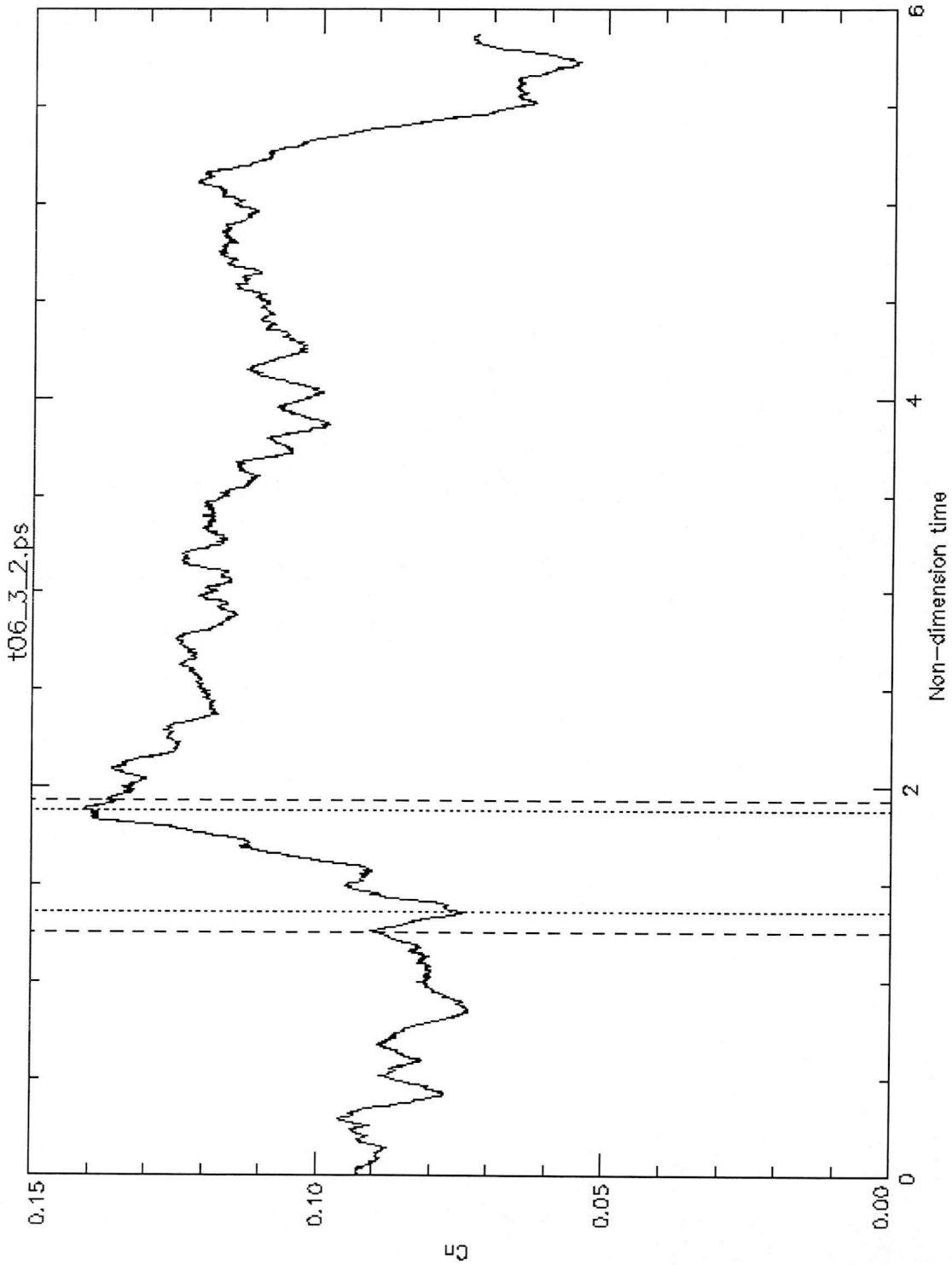

Figure 16

This figure shows the extent of a 5 % stretch of the average time period in comparison to Figures 15 and 17.
The long dashes indicate the average time period and the short dashes indicate the points taken as the start and end of the impulsive interaction with the original 'min-max'.

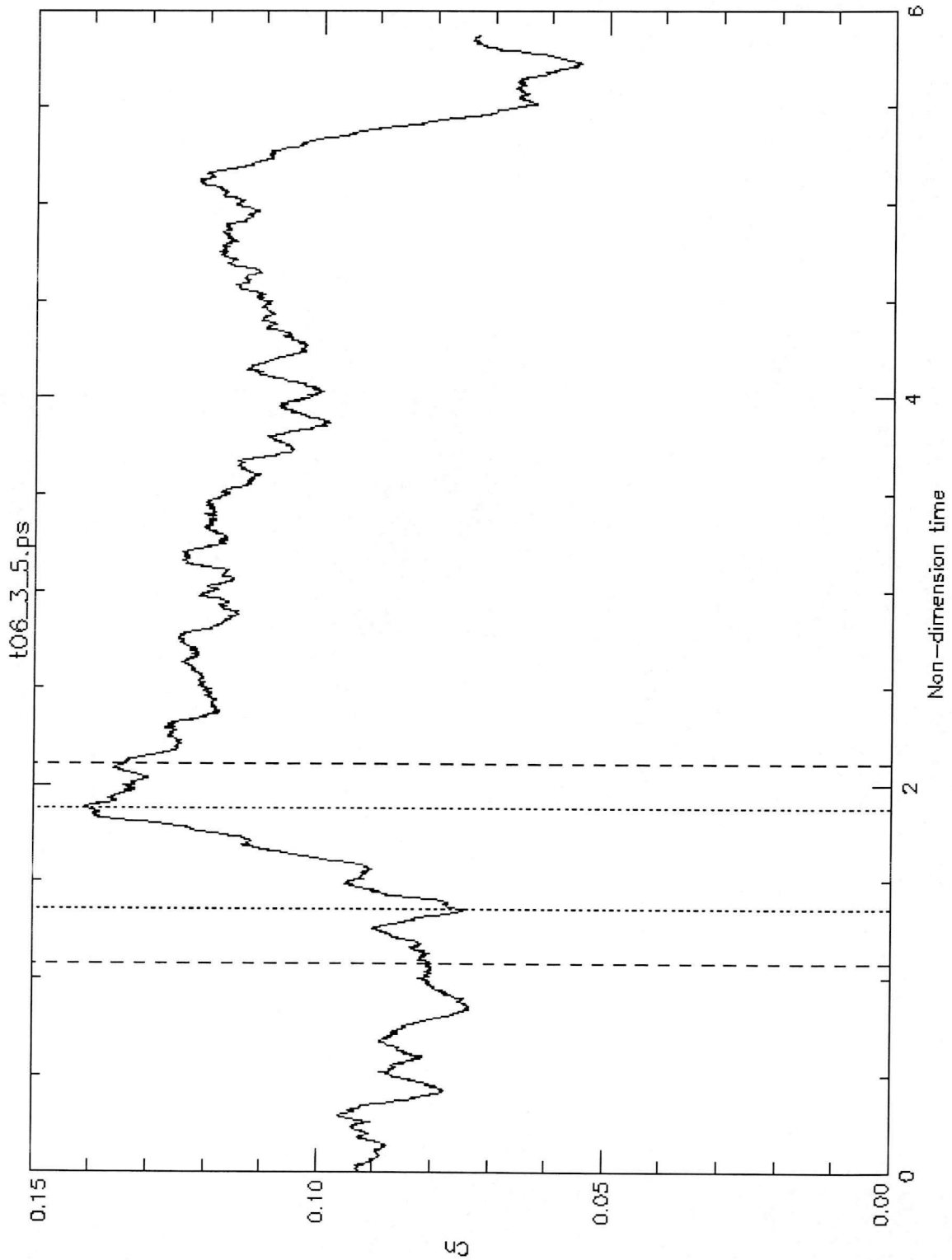

Figure 17

This figure shows the extent of a 8 % stretch of the average time period in comparison to Figures 15 and 16.
The long dashes indicate the average time period and the short dashes indicate the points taken as the start and end of the impulsive interaction with the original 'min-max'.